A New Fault-Tolerant Switched Flux Machine With Hybrid Permanent Magnets

Qian Chen, *Member*, *IEEE*, Stephen Eduku, and Wenxiang Zhao *Senior Member*, *IEEE*

Abstract— **This paper put forward a new fault-tolerant hybrid switched-flux PM (HSFPM) machine design employing the synergy of NdFeB and Ferrite Magnet. The key of the proposed HSFPM designed machine is the unique design E-core laminated stator with the hybrid magnet to ensure a drastic reduction of NdFeB magnet without compromising the output performances and efficiency in the conventional SFPM machine design to avert the huge demand of NdFeB and its associated volatile high price increase. Additionally, the fault-tolerant stator teeth designed principle implemented in the proposed HSFPM machine provides enhanced segregation among the various phases and ensures continuity of operation with acceptable operating performance under fault-condition. For fair evaluation and comparison, both the proposed HSFPM and the conventional SFPM (CSFPM) machine have the same slot-pole combination, winding arrangements, and stator/rotor dimensions except for the unique outer-stator of the proposed design. Meanwhile, compared to the CSFPM machine, the proposed HSFPM machine design makes use of only 60% of the PM (NdFeB) length. Finally, the evaluation of the no-load in conjunction with the load condition performances was carefully investigated by the Finite Element Method (FEM) of the ANSYS Maxwell software. The results depicted that the proposed HSFPM exhibits similar sinusoidal back electromotive force, comparable output torque, and slightly higher efficiency compared to that of the CSFPM machine.**

Index Terms—**Fault-tolerant, Hybrid Switched-Flux PM (HSFPM), Ferrite, Neodymium (NdFeB), E-core laminated Stators.**

I. INTRODUCTION

PERMANENT magnet machines with magnets presented in their rotor structure, which is popularly known as rotor-PM machines as well as the switched reluctance machines have been technologically advanced in recent years. Nevertheless, the switched reluctance machines continue to suffer comparatively lower power density, whereas the rotor-PM designed machines still exhibit week mechanical designed structure [1]. Hence, in [2] a novel brushless PM machine in which the PMs are placed or installed in the stator with an acronym stator-PM machine has been developed, which exhibit or present a higher power density and a higher level of mechanical integrity as the merit of the design. However, it is worthy to highlight that the switched-flux PM machine can be considered among the novel concept of an electrical machine design that offers unique superiorities over its counterpart, the conventional designed rotor-PM synchronous machine of which some of the merits pointed out is high output torque density, enhanced rotor robustness, and better efficiency [3], [4]. Nevertheless, the main economic limitation of the SFPM machines is their comparatively weaker PM usage or utilization [4]. Additionally, the SFPM designed machine has been recognized to exhibit some degree of fault-tolerant without having physical and magnetic segregation capabilities, therefore reducing the quality of the fault-tolerant operating performance of the machine [5]. Hence, it is imperative in a research point of view to enhance or improve the fault-tolerant operating capabilities of the SFPM designed machine. However, one imperative highlighted demerit cited regularly in fault-tolerant SFPM machine design is the voluminous utilization of the predominant magnet (NdFeB) and its associated high-cost [6-10]. Additionally, to figure out unique and alternative methods to ensure a substantial or significant reduction of rare-earth higher-performing permanent magnet content employed in the CSFPM machine design while sustaining the performance such as mean torque, efficiency and power density capabilities of SFPM machines has emerged in recent years as a very competitive research area, owing to the expensive and volatile price increase in permanent magnet namely neodymium (NdFeB) [11], [12]. In general design principle, there are cited three dynamic ways or manner to circumvent the aforementioned problem and these are (a) design modification aimed at enhancing the usage of PM, (b) concept of free rare-earth design, and (c) electrical excited (DC EE) design system. However, a significant enhancement in PM utilization may be obtained through design modification, with key emphasis on structural design modification and carefully sizing optimization [4]. Afrinowi *et al*. analyzed the use of a different permanent magnet (PM) in SFPM machine design [13], which demonstrates that the ferrite magnet SFPM machine produces a lower mean torque output, compare to NdFeB SFPM designed machine. However, the synergy of the ferrite and NdFeB magnet is a unique alternative solution to obtain a comparable torque density and other performances, compared to using a voluminous NdFeB magnet. Besides, owing to the drastic or significant increase in price and hug

Manuscript was submitted for review on 19, April, 2020.

This work was supported in part by the National Natural Science Foundation of China (51707083) and by the Priority Academic Program Development of Jiangsu Higher Education Institutions. (Corresponding author: Wenxiang Zhao)

The authors are with the School of Electrical and Information Engineering, Jiangsu University, Zhenjiang, 212013, China (e-mail: chenqian0501@ujs.edu.cn; stephen.eduku@yahoo.com; zwx@ujs.edu.cn).

Digital Object Identifier 10.30941/CESTEMS.2020.00012

demand of rare-earth permanent magnet (PM) elements, electric machine (motor) design with minimal rare-earth PM, weaker cost-effective ferrite magnet or no element of PM was proposed in [14], [15] while sustaining the great performances namely, high efficiency, torque density, etc., which rare-earth PM (NdFeB) designed machines can present or offer. Nevertheless, a comprehensive and detailed comparative research work in SFPM machine is carryout in terms of electromagnet capabilities or performance using various design topologies namely E-core, C-core and multi-tooth stator construction aimed at minimizing rare-earth element (PM) utilization in switched-flux designed machines, and the results established that E-core laminated constructed switching flux PM (SFPM) machine unveil the highest mean torque. Meanwhile, the E-core stator presents a relatively high torque ripple [16]-[20]. Additionally, the CSFPM designed machine presents a serious saturation region in the laminated stator teeth, owing to the coexistence of the PM and the armature conductors in the designed stator-core [21]. Hence, it is imperative to design a special E-core stator, which not only ensures a significant reduction of rare-earth PM, with a good mean torque output but also minimized the torque ripple and the serious saturation in SFPM machine design. Additionally, from the aforementioned analysis, the utilization of the hybrid PM and the structural design modification is a technological advance and pretty great technique in SFPM machine design.

In this paper, a new fault-tolerant hybrid switched-flux PM (HSFPM) machine using the synergy of ferrite and NdFeB magnets is proposed to ensure significant reduction of the predominant magnet (NdFeB) and it associated high cost in switched-flux design machine to produce a tremendous performance such as mean torque and efficiency relative to NdFeB SFPM Machine. The organization of the various sections in this paper is as follows: In section II of this paper, the design topology, slot-pole combination and winding analysis of the two aforementioned SFPM machine design will be presented. The optimization of the proposed design will be investigated in section III to ensure clarity. In section IV, the electromagnetic performance and comparison of the two SFPM design machines will be treated or investigated with the aid of the finite element method (FEM) to demonstrate or unveil the effectiveness, or the capacity of the proposed design in terms of mean torque output, losses, efficiency, and torque ripple. Lastly, the conclusions of this paper will be stipulated in section V.

II. Topology Analysis and Slot-Pole Combination

The two design topologies of the fault-tolerant SFPM machines are presented in Fig. 1, the fault-tolerant HSFPM machine is identical to that of the designed conventional SFPM machine in terms of the E-core stator, rotor structure, and the winding arrangements. However, as shown in Fig.1, compared with the conventional SFPM, the Ferrite permanent magnet (FPM) and NdFeB permanent magnet (NPM) are combined and employed in the fault-tolerant HSFPM, and the auxiliary stator is added outside the conventional SFPM. The FPM is introduced in the HSFPM machine, with air-gap segregation between the FPM and the NPM to ensure that the flux produced by the FPM contributes effectively to the production of the torque output rather than short-circuiting the stator core. Additionally, the air-gap between the FPM and NPM ensures flexibility of adjusting the hybrid PM to archive an optimal torque output, compared with the conventional SFPM machine.

To obtain good torque performance, e.g., mean torque and torque ripple, the slot-pole combination and the winding arrangement are very important. Since the period of the permanent magnet torque ripple or even the reluctance torque ripple is the same with the cogging torque period. Meanwhile, cogging torque frequency when increases, has a significant influence of decreasing the torque ripple because the magnetic power produced is changing or transforming more smoothly, particularly around the air-gap, hence, it is great importance and beneficial to ascertain a combination of higher feasible LCM(Qs, 2p). The cogging torque frequency can be stipulated as in [25]:

$$fcogging = LCM(Qs, 2p) \tag{1}$$

where Q_s and $2p$ are the numbers of stator slots and total rotor poles respectively, and the acronym LCM represents the least common multiple.

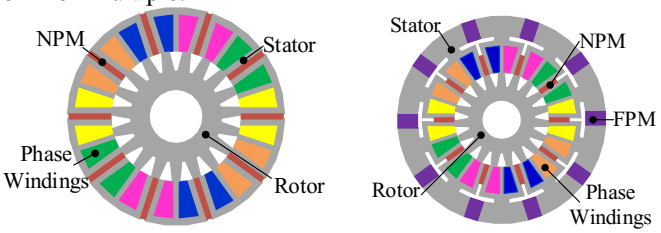

Fig. 1. Design topology of the two SFPM machines. (a) Conventional SFPM machine. (b) Proposed HSFPM machine.

The main harmonic analysis of a winding factor as given or presented in [24] and [26] is as follows:

$$k_w = k_d k_p \tag{2}$$

where k_w is termed as the main harmonic winding factor, k_d and k_p are designated as the distribution factor and pitch factor of the main harmonic respectively. For fractional-slot analysis, the pitch factor can de deduce from the equation

$$k_p = \sin\frac{\sigma_\omega}{2} \tag{3}$$

Where the span angle of the winding is denoted by the symbol $\sigma_\omega = (2\pi p y_q)$. In considering different harmonic orders, the order v of the harmonic ought to be employed in place of σ_ω instead of the parameter p.

$$k_d = \begin{cases} \dfrac{\sin\left(\dfrac{\alpha_{ph}}{2}\dfrac{\alpha_{ph}}{2}\right)}{\dfrac{q_{ph}}{2}\sin\left(\dfrac{\alpha_{ph}}{2}\right)} & \text{1f } q_{ph \text{ is}} \text{ even} \\ \dfrac{\sin\left(q_{ph}\dfrac{\alpha_{ph}}{4}\right)}{q_{ph}\sin\left(\dfrac{\alpha_{ph}}{4}\right)} & \text{If } qph \text{ is odd} \end{cases} \tag{4}$$

The feasibility of the coil, based on Q_s and p is determined

by the formula Q_s/mt and acceptable when the result is an integer and the t which represents the designed machine periodicity is derived from t=GCD(Q_s, p). Additionally, the angle that exists between two designed spokes is obtained from the formula $\alpha_{ph}=\alpha_s t/p$ where α_s denote the electrical angle. After a careful calculation and detailed analysis of the slot-pole combination, it was found out that the two selected slot-pole combination has an identical value, except for the winding factor and the LCM. However, the 10-stator slot and the 19-rotor pole is selected for both the conventional SFPM and the proposed HSFPM machine in this paper because, the 10-slot and the 19 rotor-pole prove to have the capacity to reduce the cogging torque as compare to the 10-slot and 18-pole design which has a very low LCM, albeit it has the highest winding factor. Also, it is tested and verified in [27], that the 10-slot and the 19-pole combination have a unique advantage of producing symmetrical back electromotive force, hence causing a reduction in cogging torque, whereas, the 10-slot and 18-pole produce a very serious harmonic distortion. Hence, the star of slot diagram of both CSFPM and the proposed HSFPM machine is given in Fig. 2.

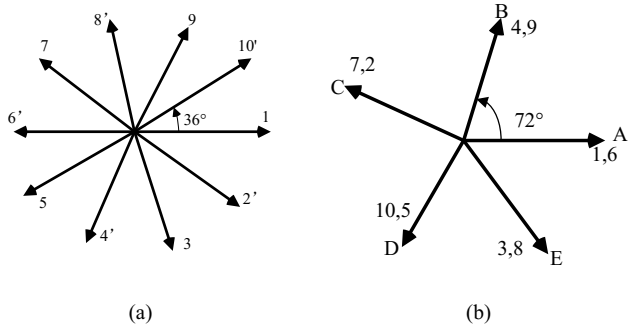

Fig. 2. The star of slot diagram of the design of the 10-slot and 19-pole. (a) The vectors of back electromotive force windings (b) The phase winding arrangement.

III. Optimization for HSFPM Machine

The optimal design for the conventional SFPM machine has been given in Ref. [27], and the initial parameters of the two SFPM machine is listed in Table I. Fig. 3 gives the detailed parameters of the two SFPM machines. To show or demonstrate the effectiveness of reduction of the NPM volume in HSFPM machine, a factor of the PM length (k_{pm}) can be presented or expressed as:

$$kpm = \frac{hpm}{\left(\frac{Dso}{2} - \frac{Dsi}{2}\right)} \tag{5}$$

where the outer and inner diameter of the SFPM machine stator is denoted as the symbol *Dso* and *Dsi* respectively as depicted in Table I.

The detailed design optimization principle of the proposed HSFPM machine will be presented in this section. Also, it is worthy to highlight that the Finite-Element method is known to be the most practical and precise design method widely employed in modeling when it comes to electrical PM machine design [4]. However, for effective optimization and comprehensive analysis of the proposed HSFPM machine using the CSFPM machine as the baseline, the search-based optimization principle, through structural design modification which depicts a series of iteration techniques to ascertain or search an optimal value or solution of an electric machine, combine with FEM is employed. Firstly, it is imperative to highlight that apart from the structural design of the HSFPM machine, the key optimization parameters of the proposed design are the hybrid magnets, with the NdFeB as more sensitive compared to that of ferrite PM. Secondly, the initial design parameters definition of both topologies as depicted in Fig. 3 are given in Table II with Model I as the baseline parameters of the CSFPM design and Model II as the HSFPM design parameters. However, for clear analysis and easy replication of the proposed HSFPM design, the four iterative set values used in the optimization process to obtain the optimal design parameters are given in Table III. The initial design optimization parameters of the HSFPM machine which are stipulated under Model II of Table II and designated as Step I values in Table III are the first search-based (iteration) of the optimization process, which unveiled the highest torque ripple with the lowest mean torque output as presented in Fig. 4(a) and Fig. 4(b) respectively. However, for clarity purposes, the values of the torque ripple and mean torque obtained from the first iteration are 10.55% and 5.78Nm respectively. In Step II, the torque ripple is tremendously reduced, whereas the mean torque, is improved, indicating some degree of success in the optimization technique as depicted in Fig.4(a) and (b) respectively. Thus the second iteration responded with a 75.45% decrease in torque ripple and a 6.92% increase in mean torque of Step II, compared with Step I. additionally, the obtained torque ripple and mean torque values are 2.59% and 6.18Nm respectively. However, the aforementioned optimization trend continues through Step III with a torque ripple of 2.89% and a mean torque of 8.99Nm, corresponds to an 11.58% increase in torque ripple and 45.47% increase in mean torque, compared to Step II. However, the visual analysis to buttress the optimization of Step III can also be seen respectively in Fig. 4(a) and (b). Finally, the iterative optimization at Step IV presents a torque ripple of 2.31% and a mean torque of 9.11Nm, corresponding to a 20% decreased in torque ripple and a 1.34% increase in mean torque, compared to Step III. However, the optimal values of the proposed fault-tolerant HSFPM machine are obtained in Step IV due to its significant torque ripple reduction and an improved mean torque output compared to all the various steps of the optimization process as presented respectively in Fig. 4(a) and (b). Additionally, it is imperative to highlight that, the Step IV iterative values presented in Table III is chosen as the optimal design parameter values of the HSFPM because, compared with the CSFPM machine, the HSFPM design exhibit pretty much comparable mean toque, torque ripple reduction, and slightly higher efficiency. Meanwhile, all the various steps of the optimization process are depicted in Fig.4 (a) and (b) to enhance the aforementioned optimization analysis. However, it is imperative to point out that, some structural design parameters of the proposed design were kept constant with the CSFPM design during the optimization process. Additionally, the final optimal values are given in Table IV.

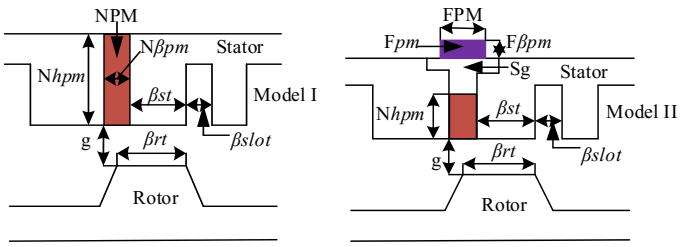

Fig. 3. Detail parameters of two SFPM machine. (a) Conventional SFPM machine (b) Proposed HSFPM design.

TABLE I
DESIGN PARAMETERS (SPECIFICATION) OF THE TWO SFPM MACHINES

Symbol	Parameters	Model I	Model II
D*so*	Stator outer diameter (mm)	145	190
D*si*	Stator inner diameter (mm)	87	87
D*ro*	Rotor outer diameter (mm)	86.2	86.2
D*ri*	Rotor inner diameter (mm)	36	36
La	Active axial length (mm)	60	60
g	Air-gap length (mm)	0.4	0.4
Nr	Rated speed (r/min)	1500	1500
Ia	Rated current (A)	4.1	4.1
N*Br*	NdFeB PM remanence (T)	1.2	1.2
F*Br*	Ferrite PM remenance (T)	0	0.4
N*t*	Number of turns per slot	70	70
M	Number of phases	5	5
	NdFeB PM material	NdFe35	NdFe35
	Ferrite PM material	-	Y30

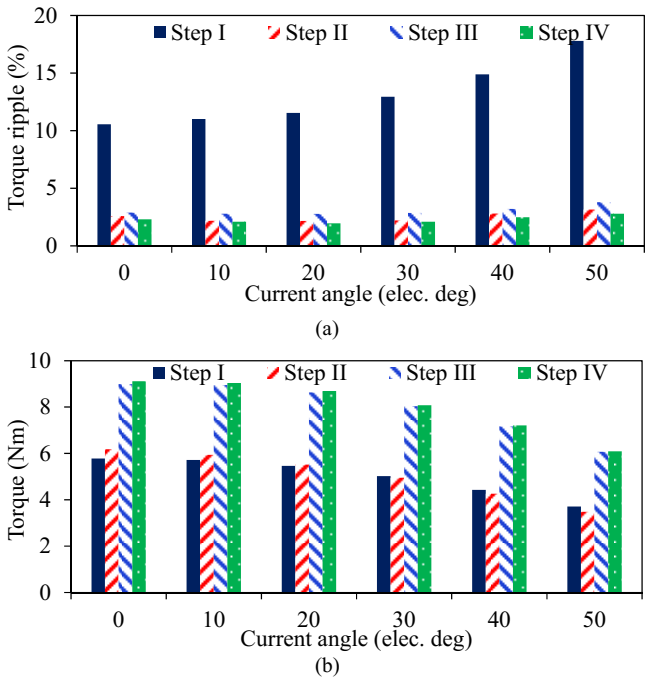

Fig.4. Optimization analysis of the proposed HSFPM design. (a) Torque ripple waveform. (b) Mean torque waveform of the design.

TABLE II
INITIAL OPTIMIZATION SET PARAMETERS FOR BOTH DESIGNS

Symbol	Parameters	Model I	Model II
β*st*	Stator tooth width (deg)	16.92	16.92
β*slot*	Stator slot width (deg)	6.66	6.66
β*rt*	Rotor pole arc (deg)	6.96	6.96
N*hpm*	NdFeB PM length (mm)	28.01	25.03
N*βpm*	NdFeB PM width (mm)	3.29	5.03
F*hpm*	Ferrite PM length (mm)	-	18
F*βpm*	Ferrite PM width (mm)	-	10

TABLE III
ITERATIVE SET VALUES FOR THE HSFPM OPTIMIZATION OF THE FOUR STEPS

Item	N*hpm*(mm)	N*βpm*(mm)	F*hpm*(mm)	F*βpm*(mm)
Step I	25.03	5.03	18	10
Step II	14.01	4.37	18	15
Step III	18.01	3.63	18	12.25
Step IV	15	3.63	18	14

TABLE IV
PARAMETERS AFTER PROPOSED DESIGN OPTIMIZATION

Symbol	Parameters	Model I	Model II
β*st*	Stator tooth width (deg)	16.92	16.92
β*slot*	Stator slot width (deg)	6.66	6.66
β*rt*	Rotor pole arc (deg)	6.96	6.96
N*hpm*	NdFeB PM length (mm)	28.01	15
N*βpm*	NdFeB PM width (mm)	3.29	3.63
F*hpm*	Ferrite PM length (mm)	-	18
F*βpm*	Ferrite PM width (mm)	-	14

It is worthy to emphasize that compared to the conventional designed SFPM machine, only 60% of the NPM length is employed, thus *kpm*=15/25 in the proposed HSFPM machine. Hence, the influence or effect of the Ferrite magnet is very obvious and easily noticed. As presented in Table II and IV, the parameters such as *βst, βslot, βrt,* and other parameters of both machines are kept constant (same) to enable a fair comparison. Nevertheless, it is worthy to highlight that, there is a 68.37% reduction in PM volume in the proposed design compared to the conventional SFPM design.

IV. ELECTROMAGNETIC PERFORMANCE AND COMPARISON

A. No-load Performances

The key characteristics of the no-load operating condition analyzed in this section of this paper are flux-density distribution, air-gap flux density, flux-linkage, back EMF, and cogging torque. However, the aforementioned characteristics are systematically reported or demonstrated clearly from Fig. 5 to Fig. 9. Firstly, the reduction of the magnetic field presented in the HSFPM as compare to the conventional SFPM machine is due to the reduction of the volume of NdFeB magnet in the HSFPM machine. The computation of the flux density, as well as the field distributions of the two design obtained from the 2-D FEM method of ASYS-Maxwell software, are shown in Fig. 5. As depicted in Fig. 5, the peak or the maximum flux density values are 1.75T and 1.73T respectively. Hence, it signifies that the HSFPM might have a slightly lower back electromotive force (back-EFM). Additionally, it should be highlighted that the saturation region of the conventional SFPM designed machine is larger than that of the proposed HSFPM machine.

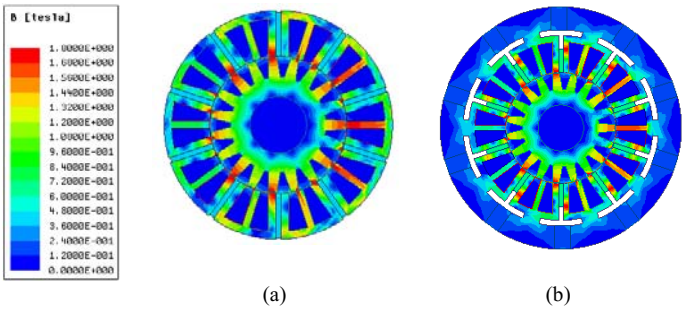

Fig. 5. Flux density distribution. (a) Conventional SFPM Machine. (b) HSFPM machine.

As demonstrated clearly in Fig. 6 (a) and (b), both radial and circumferential induced air-gap flux density of the two SFPM design have similar waveform modulation, with the CSFPM design having an infinitesimal increased in flux, as compare to the proposed HSFPM design. Nevertheless, it is imperative to highlight that the two SFPM designs have similar design parts, except for the specially designed stator in the proposed HSFPM design.

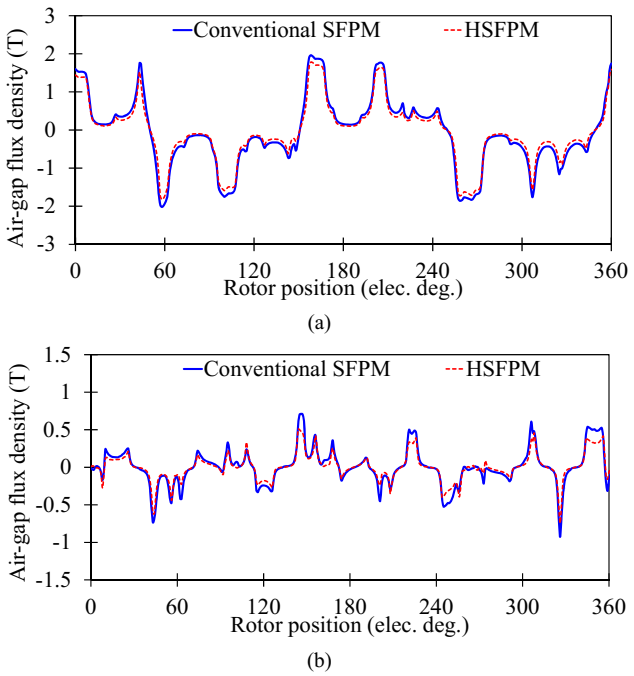

Fig. 6. Air-gap flux-density by the simulation analysis, presented in the two SFPM machines at the no-load operating condition. (a) Radial (b) Circumferential.

Fig. 7. depicts the flux-linkage waveform as well as harmonic content analysis. As can be seen in Fig. 7 (a), the two designs present or exhibits an identical flux-linkage to demystify the capacity of the proposed HSFPM machine as compare to the conventional SFPM machine. Additionally, the flux-linkage produced by the two designs (Models) is of bipolar waveforms. However, Fig. 7 (b) clearly shows that the conventional SFPM machine offers a slightly higher fundamental harmonic component as compared to the proposed HSFPM.

Fig. 8 represents the electromotive force (back-EMF) waveform and its harmonic content of phase A of the two machines at no-load condition. As can be seen in Fig. 8 (a), the waveform of the electromotive force of the proposed HSFPM design is pretty similar and sinusoidal compared to that of the conventional SFPM design. For polyphase machines, such as five-phase PM motor, the predominant or dominant causes of ripple torque generation are the 9th, 11th, 19th, and 21st order of harmonic content [28]. However, it is imperative to aim at the reduction of the above mention harmonic orders in five-phase machine design. As presented in Fig. 8 (b), the conventional SFPM design exhibit the highest FHC as compared to the proposed HSFPM design. Albeit, the 9th and 11th harmonic content increase in the HSFPH, it is worthy to highlight that the 19th and 21st order of harmonic reduces dramatically in the proposed HSFPM machine. Also, the proposed HSFPM design presents a THD of 2.8% whereas the conventional SFPM design exhibit 3.3%.

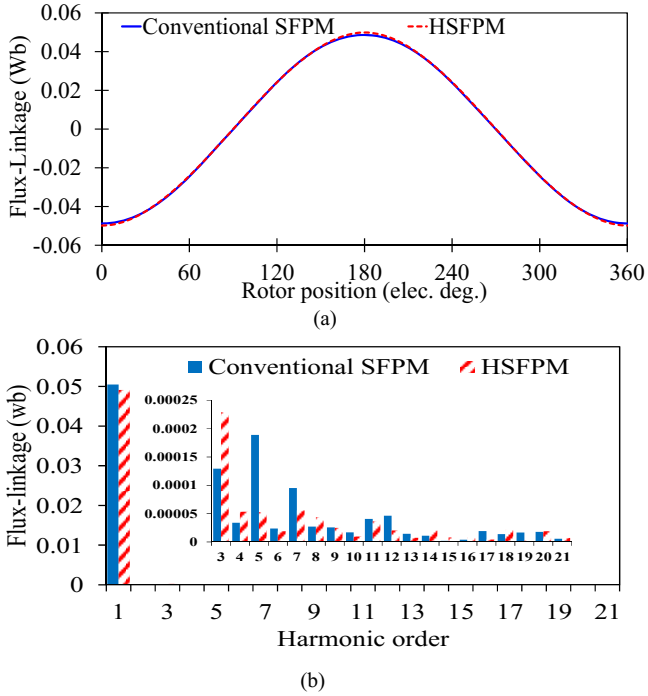

Fig. 7. No-load flux-linkage and it harmonics waveform analysis. (a) Flux-Linkage Waveform. (b) Harmonic order.

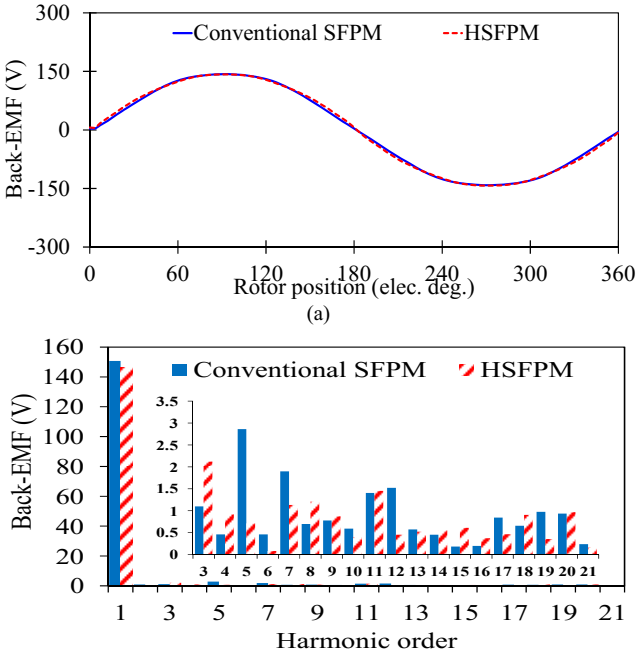

Fig. 8. No-load back EMF and its harmonic analysis at 1500 rev/min operating conditions of the two designs. (a) The waveform of the back-EMF. (b) Harmonic order waveform.

The produced waveform of Fig. 9, depicts the cogging (no-current) torque performance analysis and comparison of the SFPM machines. As highlighted in Fig. 9, it is very obvious that the cogging torque amplitude of the CSFPM machine exhibit the highest value compare to the proposed HSFPM design. However, peak-to-peak values of the CSFPM, as well

as the proposed HSFPM design, are 148mm and 100mm respectively. Hence, the cogging torque of the proposed HSFPM design is 32% lower than the CSFPM design. However, the cogging torque generated by the design has ten periods and can be computed by using (6).

$$N_E = \frac{N_{QS}}{GCD\left(N_{QS}, N_R\right)} \tag{6}$$

Where N_E, N_{QS}, N_R, and GCD are designated as the specific number of periods in a one-electrical cycle, stipulated number of the design stator poles, number of selected rotor, and greatest common factor or divisor.

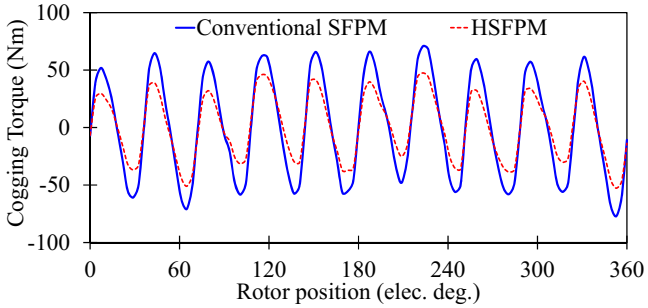

Fig. 9. Cogging torque analysis of the two SFPM design.

B. Performance Analysis of the Load Condition

The performance of the aforementioned two SFPM designed machine will be analyzed in this section with the injected current of amplitude 4.1 amperes. For clarity purposes, the waveform of Fig. 10, depicts the torque performance analysis obtained or retrieved by the 2-D FEM method. The obtained mean torque (T_{avg}) of the conventional SFPM and the proposed HSFPM machine are 9.3 Nm and 9.1 Nm respectively, and the associated torque ripples generated are 3.97% and 2.31% respectively under the current angle of 0°. However, the torque ripple T_{ripple} of the design can be established by the equation

$$T_{ripple} = \frac{(T_{\max} - T_{\min})}{T_{avg}} \times 100\% \tag{7}$$

where T_{max} and T_{min} represent the maximum and minimum value of the torque respectively. The key and imperative point to highlight in this section are that the proposed HSFPM machine exhibits or offers a comparative torque output performance as compare to that of the conventional SFPM machine. Hence, a significant reduction of the dominant rare-earth (NdFeB) magnet in the conventional SFPM machine design with appreciable reduction of the volatile high price increase of NdFeB can be attained or realized in the HSFPM design and yet sustain a good torque output.

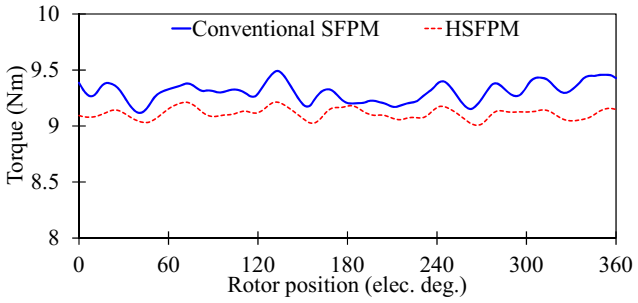

Fig. 10. Mean torque waveform.

Presented in Fig. 11, is the performance analysis of the torque angle in conventional SFPM and proposed HSFPM designs. As highlighted in Fig. 11 (a), the mean torque output of CSFPM at various current angles are slightly higher than the proposed HSFPM, this is because the line back electromotive force obtained through the optimization process of HSFPM is slightly lower than that of CSFPM. Meanwhile, Fig. 11(b) present the torque ripple waveform of the two SFPM machines, with conventional SFPM exhibiting the highest torque ripple at a various current angle. Additionally, considering the conventional SFPM and proposed HSFPM at the current angle 0°, the mean torque loss of the HSFPM machine is 0.2 Nm, which is acceptable due to the significant reduction of torque ripple in HSFPM design as compare to CSFPM design.

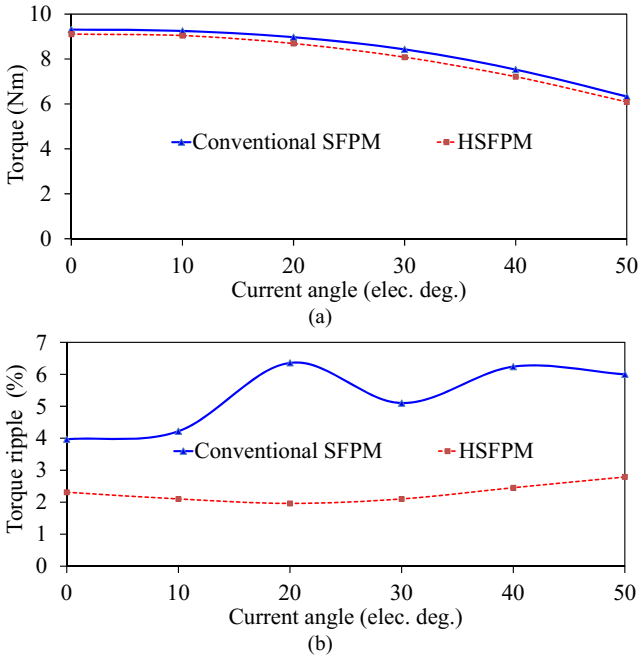

Fig. 11. Performance analysis of the torque angle of the two SFPM machines. (a) Mean torque and (b) Torque ripple.

C. Power Density Analysis and Comparison

The computed output power at the current-angle of zero degrees (0^0) of both CSFPM and the proposed HSFPM designs are 1.461kW and 1.429kW respectively. The designated outer-stator diameter of the CSFPM and the proposed HSFPM machines are 145mm and 190mm respectively with a common axial-length of 60mm. Afterwards, the computed volumes of the CSFPM and HSFPM machines are 0.99L and 1.7L respectively. Hence, as shown in Table V, the power density exhibited by the CSFPM machine is higher than that of the proposed HSFPM machine, with their values depicted as 1.48kW/L and 0.84kW/L respectively. Meanwhile, the computed loss of power density in the HSFPM design compared to that of the CSFPM design is 0.46kW/L, which is as a result of the reduction of NdFeB magnet in the HSFPM machine. Albeit, the HSFPM has a lower power density, it exhibits great superiority in terms of other imperative output performances and ensures a significant reduction of NdFeB magnet to avert its high demand as compared to the CSFPM machine.

TABLE V
POWER DENSITY COMPARISON OF THE TWO SFPM MACHINES

Items	Model I	Model II	%Decreased
Output Power (kW)	1.461	1.429	2.2
Volume (L)	0.99	1.7	-
Power Density(kW/L)	1.48	0.84	26.8

D.Iron Core Losses and Efficiency Comparison

Section D of this paper presents the iron losses with its waveforms and the computed efficiency of the two Models to enhance the comparison and unearth the effectiveness of the proposed HSFPM design. However, to demystify the aforementioned merit of the proposed HSFPM design, the waveforms of the losses are presented in Fig. 12(a) to (c) respectively. The obtained losses with the aid of the 2-D FEM, under the current angle of 0^0 are stipulated in Table VI, which depicts that the conventional SFPM design unveils the highest iron losses, compared to the proposed HSFPM. The percentage decreased in losses between the conventional SFPM and HSFPM, from the stator, rotor and PM are 7.4%, 10.3%, and 81.2% respectively from the results depicted in Table VI. Since, the PM losses in conventional SFPM design which make use of only NdFeB is 81.2% higher than that of the proposed design with the hybrid magnet, it can be concluded that the introduction of the less expensive but cost-effective magnet (Ferrite) can ensure a considerable reduction of PM losses and improve the efficiency. Additionally, the efficiency (η) of the conventional SFPM design (Model I), as well as the proposed HSFPM design, can be determined by the formula:

$$\eta = \frac{T_{avg}\omega}{T_{avg}\omega + P_r + P_{PM} + P_s + P_c} \times 100\% \quad (8)$$

where the P_{PM}, P_r, P_s, ω and P_c are designated as PM losses, Rotor iron losses, Stator iron losses, copper losses, and mean torque respectively. However, the efficiency of conventional SFPM (Model I) and HSFPM (Model II) is 95.9% and 96.5% respectively. Nevertheless, the proposed HSFPM exhibits a slightly higher efficiency compared to its conventional counterpart due to the higher losses in conventional SFPM. Hence, it can be concluded that the proposed HSFPM design is pretty effective and capable of producing a comparable output performance to that of the conventional SFPM machine employing only NdFeB.

V.CONCLUSION

In this particular paper, a new fault-tolerant HSFPM machine aimed at reducing the predominant NdFeB magnets in the CSFPM machine, yet sustaining the well-known high torque and efficiency of the CSFPM design with infinitesimal or minimal core losses and torque ripple is proposed. The results established by or obtained from the two aforementioned designs by the application of Finite Element Method (FEM) depicts that the proposed HSFPM designed machine exhibits a comparable torque output as well as slightly higher efficiency, compared to the conventional designed SFPM machine.

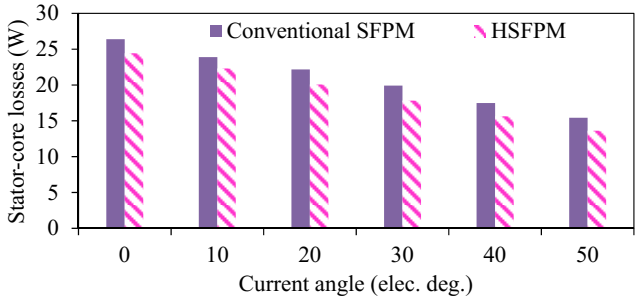

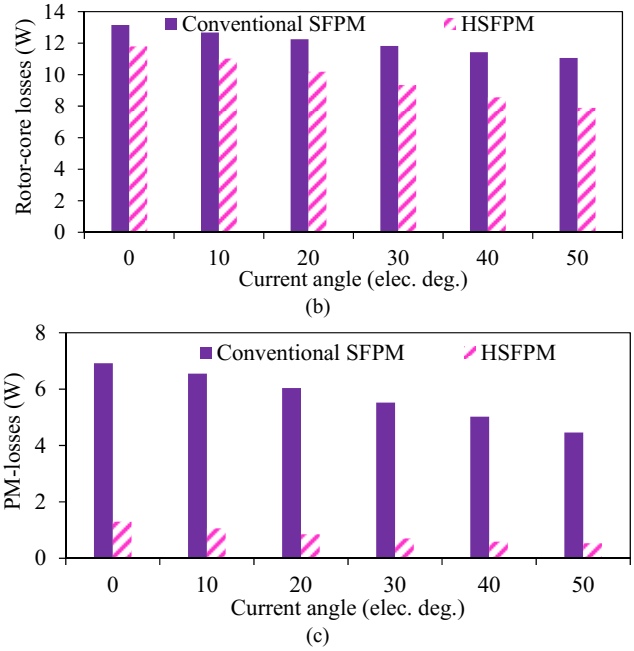

Fig. 12. Obtained core-loss waveforms of the two SFPM designed machines. (a) Stator-loss, (b) Rotor-loss and (c) PM-loss.

TABLE VI
IRON LOSS COMPARISON OF THE TWO SFPM MACHINES

Items	Model I	Model II	%Decreased
Stator iron loss (W)	26.39	24.43	7.4
Rotor iron loss (W)	13.15	11.79	10.3
PM loss(W)	6.92	1.30	81.2
Copper loss (W)	15.03	15.03	0

REFERENCES

[1] W. Zhao et al., "Stator-flux-oriented fault-tolerant control of flux-switching permanent-magnet motors," *IEEE Transactions on Magnetics*, vol. 47, no. 10, pp. 4191-4194, Oct. 2011.

[2] C. Liu, K. T. Chau, J. Z. Jiang and S. Niu, "Comparison of stator-permanent-magnet brushless machines," *IEEE Transactions on Magnetics*, vol. 44, no. 11, pp. 4405-4408, Nov. 2008.

[3] Y. Wang, L. Geng, W. Hao, and W. Xiao, "Improved control strategy for fault-tolerant flux-switching permanent-magnet machine under short-circuit condition," *IEEE Transactions on Power Electronics*, vol. 34, no. 5, pp. 4536-4557, May 2019.

[4] A. Nobahari, M. Aliahmadi, and J. Faiz, "Performance modifications and design aspects of rotating flux switching permanent magnet machines: a review," *IET Electric Power Applications*, vol. 14, no. 1, pp. 1-15, Jan 2020.

[5] M. Cheng, W. Hua, J. Zhang, and W. Zhao, "Overview of stator permanent magnet brushless machines," *IEEE Transactions on Industrial Electronics*, vol. 58, no. 11, pp. 5087-5101, Nov. 2011.

[6] I. A. A. Afinowi, Z. Q. Zhu, Y. Guan, J. C. Mipo and P. Farah, "Performance analysis of switched-flux machines with hybrid NdFeB and ferrite magnets," 2014 17th *International Conference on Electrical Machines and Systems (ICEMS),* Hangzhou, Oct. 2014, pp. 3110-3116.

[7] A. Fasolo, L. Alberti, and N. Bianchi, "Performance comparison between switching-flux and IPM machines with rare-earth and ferrite PMs," *IEEE*

Transactions on Industry Applications, vol. 50, no. 6, pp. 3708-3716, Nov.-Dec. 2014.

[8] T. Vaimann, A. Kallaste, A. Kilk, and A. Belahcen, "Magnetic properties of reduced Dy NdFeB permanent magnets and their usage in electrical machines," *Africon*, Sept. 2013.

[9] S. Li, Y. Li, and B. Sarlioglu, "Performance Assessment of High-speed Flux-switching Permanent Magnet Materials," *Electric Machines & Power Systems*, vol. 43, pp. 711-720, Mar. 2015.

[10] H. Chen, A. El-Refaie and N. Demerdash, "Flux-switching permanent magnet machines: a review of opportunities and challenges - part ii: design aspects, control, and emerging trends," *IEEE Transactions on Energy Conversion*, 2019, DOI: 10.1109/TEC.2019.2956565.

[11] T. Raminosoa et al., "Reduced rare-earth flux-switching machines for traction applications," *IEEE Transactions on Industry Applications*, vol. 51, no. 4, pp. 2959-2971, July-Aug. 2015.

[12] H. Hwang, S. Bae, and C. Lee, "Analysis and design of a hybrid rare-earth-free permanent magnet reluctance machine by frozen permeability method," *IEEE Transactions on Magnetics*, vol. 52, no. 7, pp. 1-4, July 2016, Art no. 8106304.

[13] I. A. A. Afinowi, Z. Q. Zhu, Y. Guan, J. C. Mipo, and P. Farah, "Switched-Flux machines with hybrid NdFeB and ferrite magnets," *Compel International Journal for Computation & Mathematics in Electrical & Electronic Engineering*, vol. 35, pp. pages. 456-472, Mar. 2016.

[14] I. Boldea, L. N. Tutelea, L. Parsa, and D. Dorrell, "Automotive electric proposed systems with reduced or no permanent magnets: an overview," *IEEE Transactions on Industrial Electronics*, vol. 61, pp. 5696-5711, Jan. 2014.

[15] Z. Q. Zhu, "Switched flux permanent magnet machines – Innovation continues," *International Conference on Electrical Machines & Systems,* Aug. 2011.

[16] Z. Q. Zhu, M. M. J. Al-Ani, X. Liu, M. Hasegawa, A. Pride, and R. Deodhar, "Comparative study of torque-speed characteristics of alternate switched-flux permanent magnet machine topologies*," inlet International Conference on Power Electronics*, Mar. 2012.

[17] J. T. Chen, Z. Q. Zhu, S. Iwasaki, and R. Deodhar, "A novel E-core flux-switching PM brushless AC machine," in *Energy Conversion Congress & Exposition,* Sept. 2010.

[18] J. T. Chen, Z. Q. Zhu, S. Iwasaki, and R. P. Deodhar, "A novel E-Core switched-flux pm brushless AC machine," *IEEE Transactions on Industry Applications*, vol. 47, no. 3, pp. 1273-1282, May-June 2011.

[19] J. Li, K. Wang and C. Liu, "A novel E-core hybrid-excited flux switching machine based on biased flux," in *Proc.* 2017 20th *International Conference on Electrical Machines and Systems* (ICEMS), Sydney, NSW, Aug. 2017, pp. 1-6.

[20] B. S. Lee, N. Pothi, M. M. J. Al-Ani, and Z. Q. Zhu, "Experimental study of torque and flux weakening performance of alternative Switched Flux PM machines," in *Proc.* 7th *IET International Conference on Power Electronics, Machines and Drives (PEMD 2014)*, Manchester, Jun. 2014, pp. 1-6.

[21] P. Su, W. Hua, G. Zhang, Z. Chen and M. Cheng, "Analysis and evaluation of novel rotor permanent magnet flux-switching machine for EV and HEV applications," *IET Electric Power Applications*, vol. 11, no. 9, pp. 1610-1618, Nov. 2017.

[22] W. Hua, G. Zhang, and M. Cheng, "Flux-regulation theories and principles of hybrid-excited flux-switching machines," *IEEE Transactions on Industrial Electronics*, vol. 62, no. 9, pp. 5359-5369, Sept. 2015.

[23] G. Zhang, M. Cheng, W. Hua, and J. Dong, "Analysis of the oversaturated effect in hybrid excited flux-switching machines," *IEEE Transactions on Magnetics*, vol. 47, no. 10, pp. 2827-2830, Oct. 2011.

[24] N. Bianchi and M. Dai Pre, "Use of the star of slots in designing fractional-slot single-layer synchronous motors," *IEE Proceedings - Electric Power Applications*, vol. 153, no. 3, pp. 459-466, 1 May 2006.

[25] B. Aslan, E. Semail, J. Korecki, and J. Legranger, "Slot/pole combinations choice for concentrated multiphase machines dedicated to mild-hybrid applications," in *Proc.* IECON 2011 - 37th Annual Conference of the *IEEE Industrial Electronics Society, Melbourne, VIC*, 2011, pp. 3698-3703, Nov 2011.

[26] H. Kang, L. Zhou, and J. Wang, "Harmonic winding factors and MMF analysis for five-phase fractional-slot concentrated winding PMSM," 2013 *International Conference on Electrical Machines and Systems (ICEMS), Busan*, 2013, pp. 1236-1241, Oct 2013.

[27] X. Xue, W. Zhao, J. Zhu, G. Liu, X. Zhu, and M. Cheng, "Design of five-phase modular flux-switching permanent-magnet machines for high-reliability applications," *IEEE Transactions on Magnetics*, vol. 49, no. 7, pp. 3941-3944, July 2013.

[28] K. Atallah, Jiabin Wang, and D. Howe, "Torque ripple minimization in modular permanent magnet brushless machines," in *Proc. IEEE International Electric Machines and Drives Conference, 2003. IEMDC'03., Madison, WI, USA,* 2003, pp. 370-375 vol.1.

Qian Chen (M'16) received the B.Sc. degree in electrical engineering and the Ph.D. degree in control engineering from Jiangsu University, Zhenjiang, China, in 2009 and 2015, respectively.

Since 2015, he has been with Jiangsu University, where he is currently an Associate Professor of Electrical Engineering with the School of Electrical Information Engineering. His research interests include electric machine design, modeling, fault analysis, and intelligent control.

Stephen Eduku received a B.Sc. and M-Tech degree in Electrical and Electronics Engineering from the University of Education, Kumasi Ghana, in 2014 and 2016, respectively. He is currently perusing a Ph.D. in Electrical Engineering at Jiangsu University, China. Since 2012, he has been with Takoradi Technical University, where he is currently a Lecturer with the Electrical and Electronics Engineering Department. His research interests and teaching include design and control of permanent magnet machines, power electronics and drives.

Wenxiang Zhao (M'08–SM'14) received the B.Sc. and M.Sc. degrees in electrical engineering from Jiangsu University, Zhenjiang, China, in 1999 and 2003, respectively, and the Ph.D. degree in electrical engineering from Southeast University, Nanjing, China, in 2010.

He has been with Jiangsu University since 2003, where he is currently a Professor with the School of Electrical Information Engineering. From 2008 to 2009, he was a Research Assistant with the Department of Electrical and Electronic Engineering, University of Hong Kong, Hong Kong. From 2013 to 2014, he was a Visiting Professor with the Department of Electronic and Electrical Engineering, University of Sheffield, Sheffield, U.K. His current research interests include electric machine design, modeling, fault analysis, and intelligent control. He has authored and co-authored over 130 technical papers in these areas.